Design and optimization of Nano-catalytic energy cell
as a portable power source

by

Arash Baladi

A thesis submitted in partial fulfillment of the requirements for the degree of

Master of Science

in

Materials Engineering

Department of Chemical and Materials Engineering
University of Alberta

Abstract

Catalytic nanoburning (CNB) of methanol vapor using platinum nanoparticles on a thermoelectric (TE) module is a simple method for converting chemical energy into electrical power. Despite the many advantages of integrated nanoburning and thermoelectric modules, continuous power generation using this method is a challenge. CNB is a two-step process whereby platinum particles ignite the methanol, raising the particle temperature. This is followed by the auto-combustion of methanol in the region near the heated particles. When the catalyst is directly integrated with a thermoelectric generator, the capillary condensation of byproduct water at the particle-particle and particle-support interfaces progressively reduces the catalyst surface area, and in turn, lowers their catalytic activity. We show that the heat transfer coefficient value of the medium between the Pt-loaded substrate and the TE generator plays a critical role in achieving the optimum catalyst surface temperature and generated voltage by the TE device. A systematic investigation of various heat transfer media shows that very high thermal conductivity and heat transfer coefficient has a detrimental effect on power generation, as the catalyst surface temperature does not attain sufficiently high values owing to excessive conductive heat dissipation. This leads to elimination of thermal gradient, which is required when TE device is used to generate output voltage and power, and water condensation on the catalyst in case of very high conductive heat loss. Very low thermal conductivity and heat transfer coefficient are also undesirable due to poor heat transfer to the thermoelectric element, resulting in the very low output voltages and powers. Controlling the heat transfer mechanisms to the TE device can

maintain a high uniform surface temperature to eliminate water condensation while sustaining a constant thermal gradient across the TE generator. Heat conduction simulations corroborate this observation and provide predictions of the heat transfer coefficient, thermal conductivity, and thickness of the heat transfer medium that can optimize the performance of the device. We demonstrate a device having a sustained output power of ~285 mW at 1.053 V using 225 sccm flow rate of air-methanol mixture.

Preface

This thesis is the original work by Arash Baladi and a part of it going to be submitted for publication soon. The list of authors include as Arash Baladi, Ken Cadien, Sushanta K. Mitra, and Thomas Thundat. I designed the reactor setup and experimental procedure, collected the data, performed computer simulations, analyzed the results, and wrote the manuscript. The co-authors of the article are the members of the supervisory committee, who helped me to develop the idea and edited the manuscript.

Dedication

I dedicate my thesis work to my family and many friends. I dedicate it to my loving parents, Ali Asghar Baladi and Roya Tahavvory, whose support and encourages have always motivated me more to work harder, and to my brother, Ali Baladi, who has been my friend and mentor as well. Special thanks to my loving wife, Behdokht Farbod, who has been more than a wife. She has been my colleague, friend, and the main support in the entire duration of this work. She was a great accompanier. You all have never left my side and are very special.

Acknowledgment

I would like to thank my supervisor, Dr. Thomas Thundat, for giving me the valuable opportunity of working with him as a graduate student. Special thanks to Dr. Thundat and the supervisory committee members, Dr. Ken Cadien and Dr. Sushanta Mitra, for the fruitful discussions and helpful advises during the design of the experiments and interpretation of the acquired data. I also thank the NIME group members at the Department of Chemical and Materials Engineering, University of Alberta, who helped me to develop my research and presentation skills.

Special thanks to Mrs. Lily Laser, the Graduate Administrative Assistant, who was always there for all of graduate students. I will never forget her friendly supports during the admission process and then from the start to the end of the program. I am sure none of the graduate students and alumni of the CME department will forget her as well. I also would like to thank the entire staff at the Department of Chemical and Materials Engineering, for the great administrative job they do.

Table of Contents

List of Tables

List of Figures

1. Introduction

Providing clean, portable, and sustainable power for current electronic devices such as laptops and cellular phones, has been a challenge in recent years. The increasing power consumption of these devices requires better power delivery systems. Batteries, especially lithium ion batteries with power densities of 0.1-0.3 kWh/kg, are the most widely used for powering these devices. However, their relatively low power density when compared to that of light hydrocarbons such as methanol, which has a high power density of 5.6 kWh/kg, means that methanol may be the battery fuel of the future [1-5]. The need to recharge or replace discharged batteries during prolonged usage and the undesirable environmental impacts of discarded batteries, due to their toxic chemicals and heavy metals, are also of concern [1,2,6]. These drawbacks demand the development of alternate portable power sources such as direct thermal-to-electrical energy conversion using thermoelectric (TE) power generators, which are compact, lightweight, quiet, and environmentally friendly and yet can utilize the high power density achievable with a fuel such as methanol. This begs the question as to whether sufficient power can be generated from methanol combustion integrated with a TE module? The work presented here provides some conclusive evidence of generating meaningful power from such an integrated system.

The objective of this research is to generate a portable power by integration of the heat produced by catalytic combustion of methanol over Pt nanoparticles, referred here as catalytic nanoburning (CNB), and the thermoelectric power generator (TE). In this

concept, methanol vapor undergoes the spontaneous burning on the Pt nanoparticles (Pt NPs) in contact with thermoelectric material. The Pt NPs are catalysts for the burning process and turn red hot when exposed to high flow rates of methanol vapor (e.g. 1000 ml/min). The operational temperature of the catalytic nanoburning close to the nanoparticles surface is estimated to be above 1000 K (adiabatic flame temperature of methanol is 2150 K [7]), and thus, no CO_2 poisoning is expected.

The main problem associated with this integrated power sources is not getting repeatable and reliable amount of heat by CNB. The reason for this unreliability is the heat sinking effect and condensation of water byproduct on the catalyst, which kills the catalytic activity of the nanoparticles. As the curvature radii at the particle-particle and particle-substrate interfaces are expected to be very small, in range of tens of nanometers depending upon the catalyst particles size, they are the ideal sites for nucleation and condensation of water, which is produced as a byproduct of the combustion.

The theory that is being proposed to overcome this problem is to limit the conductive heat transfer from the heat source, catalyst nanoparticles, to the TE generator. The limited heat transfer results in an applied a thermal gradient, which keeps the catalyst surface hot enough to prevent the water condensation and sustain the catalytic reaction. Although the TE hot side temperature is theoretically expected to lower by limiting the conductive heat transfer, the total output power and efficiency of the integrated system will be higher due to its sustainability.

The maximum reported values of output power and efficiency to date are 450 mW and 1.1%, respectively, at relatively high flow rate of 2000 sccm, while the reported temperature difference between the hot and cold side of TE was 100°C and the hot and cold side temperatures were not reported individually [1]. The objective of the present research is to generate more than 1 V open circuit voltage, 300 mW output power, and 2% total efficiency using a fairly low flow rate of 225 sccm, while the catalyst support temperature (T_s), which is the operating temperature of the device, is lower than 80°C and the cold side temperature on TE is at room temperature, ~25°C.

Here we report on the integration of methanol CNB with a thermoelectric generator and investigate the interplay between various modes of heat loss and capillary condensation of byproduct water in order to maximize the output power from the TE module. Experimental results show that heat conduction into TE module dominates the heat loss mechanism because of its large thermal mass. Sustained heat loss results in capillary condensation of by product water at the nanoparticle interfaces with a detrimental effect. Controlling the heat conduction by using spacer materials with intermediate thermal conductivity assures higher surface temperature for maintaining catalytic activity, which eliminates capillary condensation while maintaining sufficient thermal gradient between the TE hot side (TE_h) and cold side (TE_c) for optimal and sustained power generation.

2. Literature review

2.1. Catalytic combustion of methanol over Pt nanoparticles

The catalytic self-ignition of methanol vapor [1,5,8-17] and hydrogen gas [2-6,15,18-23] over noble catalysts, such as platinum nanoparticles (Pt NPs), and the combustion of heavier hydrocarbons preheated or mixed with the previously mentioned gases, i.e. hydrogen assisted ignition of methane [23], propane [6,20,21], or butane [2,23], have already been reported. Complete combustion of methanol vapor with oxygen is a stoichiometric chemical reaction, shown in equation (1), which results in carbon dioxide and water vapor release [1,7,8,14,17,24,25]. Gas chromatography (GC) has confirmed water and carbon dioxide as major byproducts of methanol catalytic combustion, indicating near complete combustion on catalyst sites [1,8,14,17].

$$CH_3OH_{(g)} + 1.5O_{2(g)} = CO_{2(g)} + 2H_2O_{(g)} \qquad \Delta H = -676KJ\,[7] \qquad (1)$$
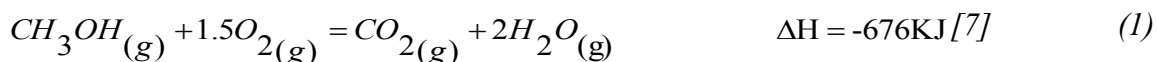
The catalytic combustion of methanol vapor using platinum nanoparticles is a two-step process. The first step involves a spontaneous catalytic exothermic reaction ($\Delta H < 0$) on Pt nanoparticles as shown in equation (1). This exothermic reaction increases the local temperature around the nanoparticles, which causes further combustion on the surface in the second step [1,2,8,9,13-15]. Depending on the design of the reactor (heat loss rate), the ratio of fuel to oxygen (heat release rate), and fuel mixture flow rate, different temperatures in the range of 300-900°C has been reported for catalytic combustion of methanol on Pt

nanoparticles [1,5,8,10-15]. At these high temperatures, the combustion reactions are expected to be complete, achieving conversion efficiency above 95% (98-99% in majority of publications) for catalytic combustion of methanol [1,2,8,9,13-15] and hydrogen [4,6,15,20,22] using Pt nanoparticle catalysts.

Therefore, methanol catalytic combustion is a potential source of continuous heat, which can generate clean electricity provided that it is properly integrated with thermoelectric generators. Heat produced by these reactions has been widely utilized for the endothermic methanol reforming processes, which requires temperature range of 250-300°C to produce hydrogen gas for portable Proton Exchange Membrane Fuel Cell (PEMFC) [3-6,11,12,14,15,18,19,26-28]. However, there are very few researches carried out on integrated CNB-TE power generators using different fuels such as methanol [1], hydrogen [6,23,29-32], butane [2,32], and propane [6]. The main challenge associated with integrating the CNB and TE generator is the large thermal mass of the TE device, which decreases the surface temperature of the catalyst [1,6,31]. Lower temperatures together with the small Kelvin radius of particle-particle and particle-support contacts results in condensation which is released as the combustion goes on [17]. Even when water vapor does not condense on the catalyst sites, the heat sink effect and reduced temperature results in poor chemical to electrical power conversion efficiencies [1,2,6,23,31,32].

Hu et al. [8] published one of the first reports on catalytic combustion of methanol over Pt nanoparticles in 2005, in which methanol-air mixture entered a reactor with Pt nanoparticles loaded on quartz wool. Pt nanoparticles (50-700 nm) were manually sprayed

over quartz wool fibers with 10 μm diameters, making a three-dimensional support with 0.1-0.5% loading. The Pt nanoparticles-loaded quartz wool was then loosely packed inside a quartz tube reactor and 1000 sccm (standard cubic centimeter) flow rate was used. They measured temperature at the center of quartz wool, using K-type thermocouples, and reported temperature as high as 600°C, which could have been higher if they used other read-out setup and thermocouples with higher measurement limit.
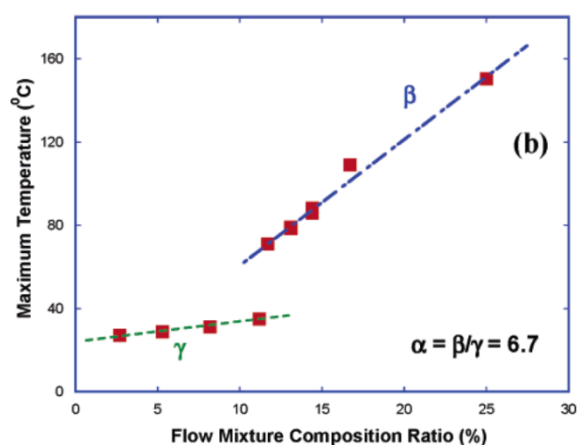
Fig. 1. Maximum reactor temperature variation flow mixture composition ratio during the catalytic combustion: γ region is a pure heterogeneous catalytic reaction and β region is a mixed heterogeneous and homogeneous (gas-phase) reaction regime [8], reprinted with permission.

It has been claimed that high temperatures in range of 600-900°C could be achieved only if enough fuel enters the reactor, resulting in methanol-oxygen molar ratio close to its stoichiometry ratio. If the molar ratio of methanol is much lower than its stoichiometry value, only heterogeneous reaction happens on catalyst sites [1,8]. Hu et al. [8] plotted the variation of maximum reactor temperature by methanol molar ratio in methanol-air mixture, which is illustrated in Fig. 1. They used a specific flow rate and recorded the maximum temperature after passing certain time, which are not clearly indicated in their paper. They mixed two flows saturated methanol-air, which came from bubbler, and dry air, which came directly from a cylinder. They named the ration of the first flow to the second one "flow mixture composition ratio" and reported lack of a homogenous reaction (gas-phase combustion) at the flow mixture composition ratio below 14%, which resulted in a very low heat output and reactor temperature (< 40°C). Increasing the methanol-air ratio to above 12.5% was reported to change the reaction regime from heterogeneous (dashed line γ) to mixed heterogeneous-homogeneous regime (dashed line β), which resulted in higher recorded temperatures.

Later in 2008, Karim et al. [1] deposited Pt nanoparticle on Al_2O_3 support (two-dimensional support) by impregnation method and studied the effect of methanol mole fraction and total flow rate on catalytic combustion of methanol, a part of which is presented in Fig. 2. Unlike Hu et al. [8], Karim et al. [1] analyzed the composition of the flow mixture of the saturated methanol-air and dry air, and they showed that heterogeneous catalytic combustion regime is sustained if low methanol-air mixture ratio (i.e. 3-4% of methanol) is employed regardless of total flow rate of mixture, which resulted in relatively

low attained temperature. Increasing the methanol mole fraction to 12.3%, which is equivalent to the O_2/methanol ratio of 1.5 (stoichiometry ratio), resulted in mixed heterogeneous-homogeneous combustion reaction and high temperatures in range of 500-650°C were recorded, depending on thermocouple position on support and total flow rate of methanol-air mixture, which is shown in Fig. 2.

As shown in Fig. 2 and 3, the higher the flow rate the higher the recorded temperature will be. The dependence of surface temperature to flow rate can be explained in two ways; first, more fuel is entering the hot reactor per unit time at higher flow rates, resulting in more combusted fuel and releasing higher amounts of heat [6]. Secondly, the O_2/fuel ratio is increased to its stoichiometry ratio at high flow rates if the bubbler is used to carry fuel and air to the reactor, and thus higher percentage of methanol molecules being combusted [13], which will be discussed later in this section.

Although catalyst surface temperature as high as 500-650°C were recorded by Karim et al. [1] when 400-1000 sccm flow rates containing 10.1-12.3% methanol was used, shown in Fig 2, the temperature profile in inlet-outlet direction is not uniform and the support surface temperature depends on thermocouple position in inlet-outlet direction. It has been shown that the first few millimeters of catalyst support in close proximity to the gas inlet develop hotspots with most of the flowing fuel combusting over this area [1,3,8,12,14,15,20,22,26,33].
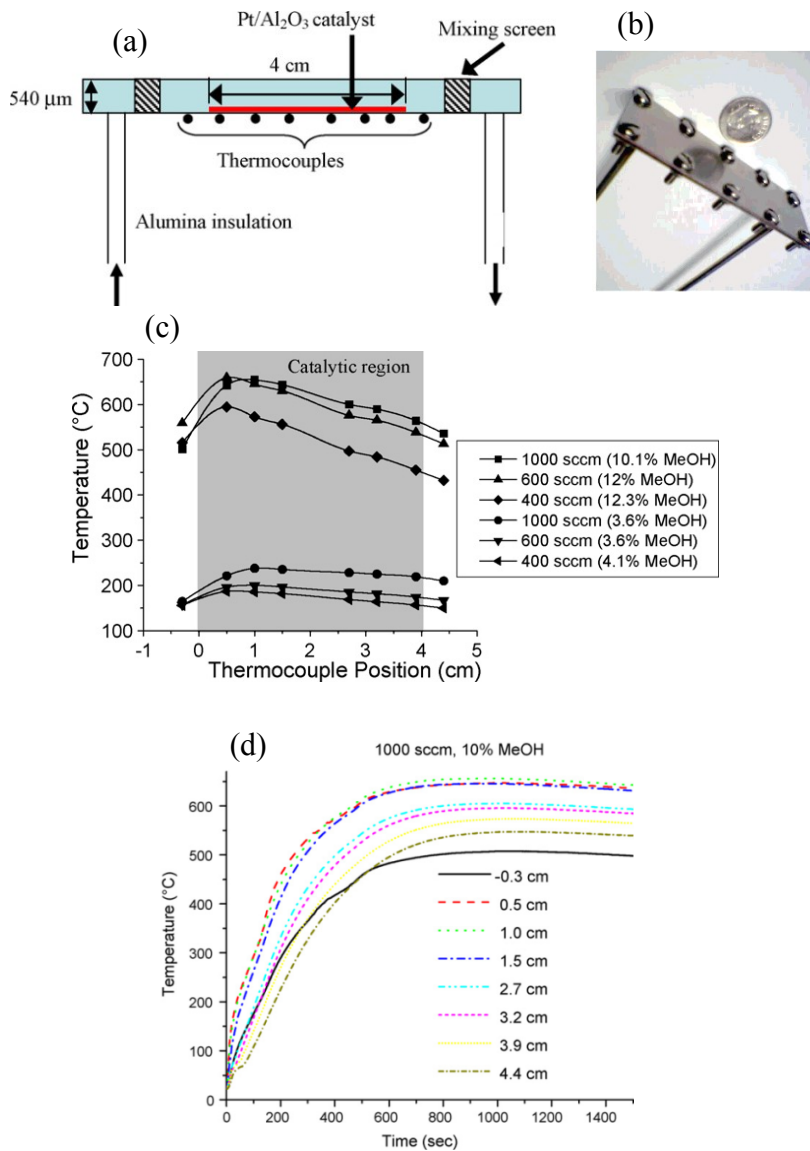
Fig. 2. (a) The schematic and (b) the real size image of the reactor that was used by Karim et al. [1]. (c) Effect of methanol-air flow rate and methanol mole fraction on steady state temperature profiles on the catalyst recorded at different distances from the inlet of the reactor. (d) Variation of surface temperature by time at different locations in inlet-outlet direction [1], reprinted with permission.
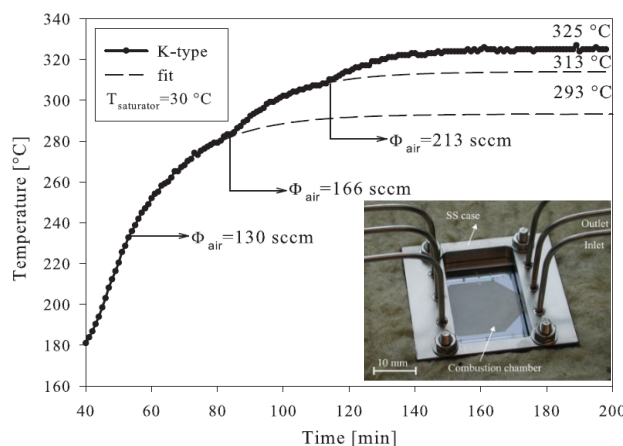
Fig. 3. Effect of air flow rate through the methanol-air flow rate on the catalyst temperature and the temperature variation variation by time when 5-8 mg of Pt (2 wt.%)–CeO2 with Pt size between 5-10 nm were coated on a Si microreactor [11], reprinted with permission.

In order to overcome this non-uniformity, Karim et al. [1] used a copper het spreader on the backside of the catalyst coated surface of the reactor. It resulted in the more uniform temperature profile in inlet-outlet direction while the maximum temperatures were decreased to 425-500°C for the same flow rates (400-1000 sccm) and methanol concentrations (8.2-11.6%), which is illustrated in Fig. 4a. Integration of the used reactor with thermoelectric generator, the cold side of which is attached to a heat sink at room temperature, did not necessarily result in the same catalyst temperature even if 2000 sccm was used and it resulted in ~100°C temperature difference between the TE hot and cold sides, which is shown in Fig. 4b. The output power is reaching ~600 mW, which lowers to

450 mW when it gets stable, resulting in 1.1% efficiency which is considered a record. Heat dissipation through the TE thickness and the heat sink that is attached to its cold side resulted in lower catalyst temperature, output power, and efficiency than expected.

(a)   (b)
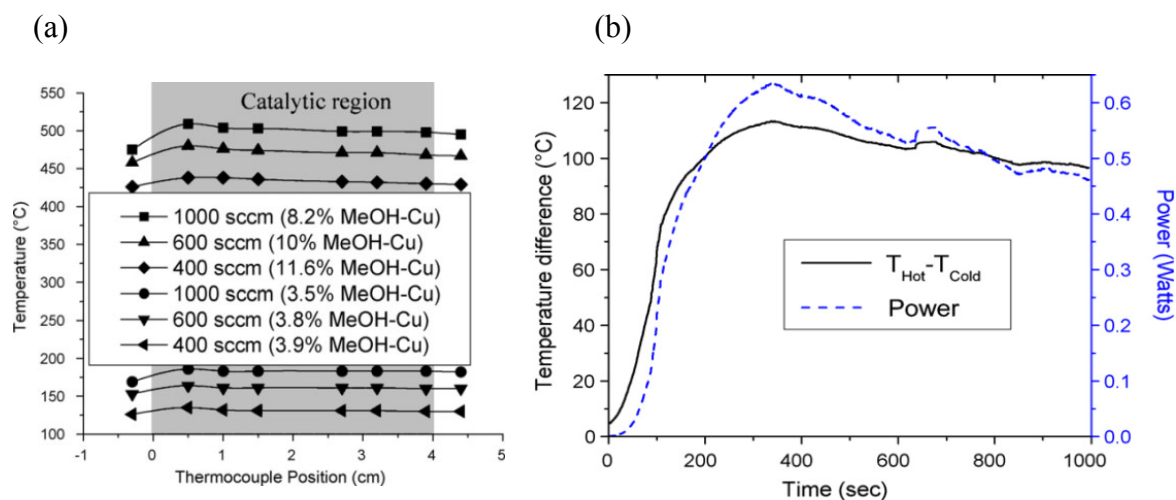
Fig. 4. (a) Effect of methanol-air flow rate and methanol mole fraction on steady state temperature profiles of the catalyst when the copper heat spreader is attached to the reactor. (b) Variation of the temperature difference between the TE hot and cold side and the output power by time [1], reprinted with permission.

Two dimensional catalyst supports (e.g. catalyst nanoparticles coated on flat or micro-channeled Si wafer) have been reported to provide lower pressure drop inside the reactor and a more uniform temperature profile on the support compared to the three dimensional ones (e.g. packed bed). This results in a higher conversion rate for 2-D supports because of

the elimination of hot spots at the inlet and the better heat transfer from these hot spots to other catalyst sites close to the outlet. Therefore, the 2-D supports provide more active catalyst sites, which catalytically combust the majority of un-reacted gasses [3,4,12].

2.2. Methanol vapor delivery

One of the most convenient ways to carry methanol vapor to the reactor, which contains Pt nanoparticle catalysts on a support, is to pass air or oxygen through a bubbler of methanol. Using a bubbler at room temperature and low flow rates, it is assumed the air is saturated with methanol vapor close to its stoichiometry ratio, which moves to the reactor then [1,8,11,13]. The computed molar ratio of oxygen to methanol at room temperature (23-24°C) is approximately 1.19, corresponding to the equivalence ratio of 1.26 [11,13]. The equivalence ratio is defined as equation (2):

$$\varphi = \frac{\left(\frac{Fuel}{Oxygen}\right)_{Experimental}}{\left(\frac{Fuel}{Oxygen}\right)_{Stochiometric}} \qquad (2)$$

As presented by Ma et al. [13], the experimental oxygen to methanol molar ratio values of 1.15, which is 0.04 lower than the computed value, has been reported for air flow speeds of lower than 5 cm/s, equivalent to flow rate of 34 sccm through the bubbler [13]. Increasing the air flow rate is expected to slightly increase this O_2/fuel ratio due to short time for air bubble to saturate with methanol vapor [1,8,11,13]. Ma et al. [13] showed how oxygen to methanol molar ratio increased to about 1.55 and equivalence ratio decreased to approximately 1 when air flow speed through the bubbler is increased to 21 cm/s, equivalent to flow rate of 143 sccm. Therefore, oxygen and methanol with near

stoichiometric ratio can be easily provided by bubbler. The use of a bubbler, moreover,

provides a simple fuel delivery system with minimum number of attached parts, favored

for portable power sources.

2.3. *Thermoelectric device and its efficiency*

Thermoelectric materials are n-type or p-type semiconductors, which are capable of converting heat to electricity and vice-versa. For this purpose, heat must be applied to one end of the thermoelectric and provide the temperature gradient in hot-cold direction. Once the thermal gradient is imposed on a thermoelectric material ($\Delta T = T_H - T_C$), the potential difference (V) is generated in order to keep the chemical potential of charge carriers uniform throughout the material. Thermoelectric materials are ranked by a Figure of merit, zT, which is defined as equation (3) and depends on electrical conductivity (σ), square of Seebeck coefficient (*S*), temperature (*T*), and reciprocal of thermal conductivity (κ) of the employed thermoelectric material. Seebeck coefficient is defined as the ratio of generated voltage (*V*) to applied temperature gradient (ΔT) [34-38].

$$ zT = \frac{\sigma S^2 \, T}{\kappa} \qquad (3) $$

Higher electrical conductivity and Seebeck coefficient as well as lower thermal conductivity (to maintain thermal gradient along TE) are highly desired for increasing the zT value of the TE material. Many researchers are specifically working on thermoelectric materials to either develop new materials or improve the zT of current materials. The higher the zT value, the higher the efficiency of TE device (η_{TE}), which is calculated by equation (4) [32,38]:

$$ \eta_{TE} = \frac{T_H - T_C}{T_H} \cdot \frac{\sqrt{1+z\overline{T}} - 1}{\sqrt{1+z\overline{T}} + \left(\frac{T_C}{T_H}\right)} \qquad (4) $$

where T_H, T_C, and $\bar{T}$ are the hot side, cold side, and average temperature (in Kelvin) on the TE, respectively.

Thermoelectric power generators, referred as TE modules, are made of pairs of n- and p-type semiconductors, referred as TE legs, which are electrically connected in series and thermally connected in parallel. The schematic of a TE module is presented in Fig. 5. When a temperature gradient is established through the TE legs, the electrons and holes, which are charge carriers in n-type and p-type semiconductor legs, respectively, start to migrate from hot to cold side of these legs in order to balance the chemical potential of the charge carries in hot-cold direction. Tendency of charge carriers to diffuse to cold side results in a net charging at cold ends of all embedded legs, which is negative in case of n-type legs and positive for p-type ones. Therefore, the electrostatic potential difference (voltage) is established through the legs. This is called Seebeck effect, which requires an equilibrium state between diffusion of charge carriers to the colder side of TE due to chemical potential and electrostatic repulsion due to accumulation of charges at cold end. The temperature difference provides the voltage of V = SΔT from the Seebeck effect (S is the Seebeck coefficient) while the heat flow drives the electrical current, which therefore determines the power output. In order to maintain the thermal gradient through the TE legs, the cold side must be in contact to a heat sink [34-38].
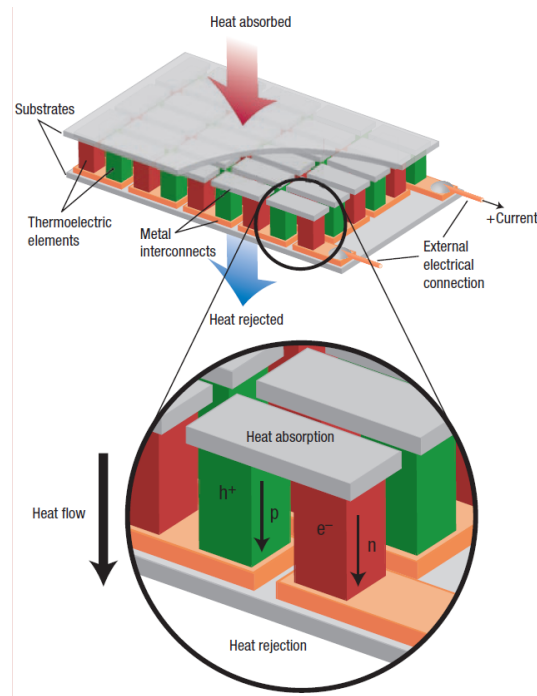
Fig. 5. Schematic of a thermoelectric module showing the direction of the heat transfer and charge flow [38], reprinted with permission.

The plots of ZT variation by temperature for some n-type and p-type TE materials are presented in Fig. 6 (a) and (b), respectively. The highest ZT values for most common TE materials are typically in the range of 0.8 to 1.1. The most widely used thermoelectric materials for low temperature applications (< 200°C) are Bi_2Te_3 and Sb_2Te_3 alloys, and the most common n-type and p-type compositions are near $Bi_2(Te_{0.8}Se_{0.2})_3$ and $(Sb_{0.8}Bi_{0.2})_2Te_3$, respectively. For high-temperature (> 650°C), silicon–germanium alloys are typically used for both n- and p-type legs [36-38].
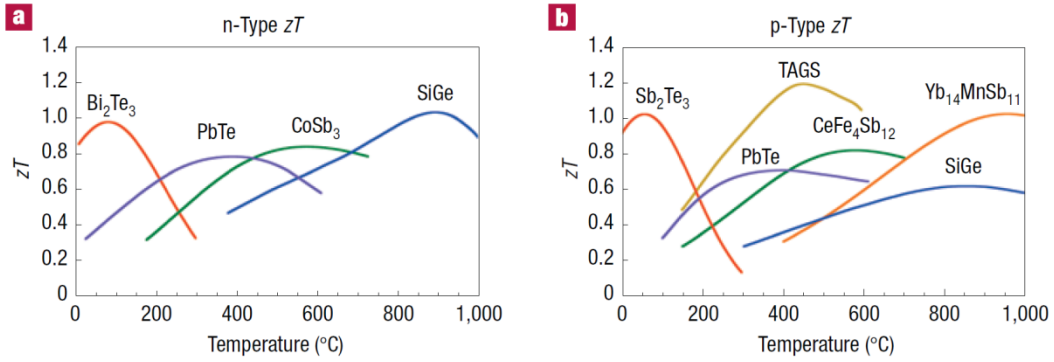
Fig. 6. Figure of merit (ZT) variation by temperature for some of the commercial thermoelectric materials used or being developed for power generation applications: a) n-type, and b) p-type. Most of these materials are complex alloys with dopants, and approximate compositions are shown here [38], reprinted with permission.

The zT value of the most of the commercially available thermoelectric materials, either n or p-type, are between 0.8-1.1, which makes the thermoelectric devices work below ~10% efficiency [36-38]. The variation of η_{TE} with temperatures is represented in Table I, and the given zT values are based on average values for Bi_2Te_3 and Sb_2Te_3 thermoelectric compounds used in commercially available TE devices [38]. Based on the temperature examples in Table I, the thermoelectric efficiency is estimated at $\eta_{TE} = 9.9\%$ when operation temperatures are $T_H = 300\ ^\circ C$ and $T_C = 50\ ^\circ C$, and reducing the temperatures to $T_H = 150\ ^\circ C$ and $T_C = 35\ ^\circ C$ results in a drop in the efficiency to 6.4%. The thermoelectric efficiency is estimated at 3.0% if the temperatures are further reduced to $T_H = 70\ ^\circ C$ and

$T_C = 25\,°C$. Therefore, the thermoelectric efficiency of the given TE depends on the operation temperatures and we have no control over it unless by maximizing the thermal gradient across its thickness. The maximum operating temperature of the used TE device is $T_H = 320\,°C$, which may result in $\eta_{TE} = 11.5\%$ if the cold side is kept at room temperature ($T_C = 25\,°C$).

Table I. Examples of the variation of η_{TE} with operation temperatures (the given zT values are estimated based on average values for Bi_2Te_3 and Sb_2Te_3 compounds)

$T_H\,(°C)$	$T_C\,(°C)$	$z\bar{T}$	η_{TE}
300	50	0.8	9.9
250	45	0.85	9.2
200	40	0.85	7.8
150	35	0.9	6.4
100	30	0.9	4.4
85	25	0.9	3.9
70	25	0.9	3.0

3. Experimental and simulation methods

A CNB power generator was fabricated using a commercially available square (30×30 mm) TE module with the top and bottom surfaces covered by graphite foil , which has a thermal conductivity of 1.75 W/(m.K) across its 3.75 mm thickness (1261G-7L31-04CL, Custom Thermoelectric Inc., USA). The TE module was placed in a disk-shaped CNB reactor which has a 7 cm inner diameter and 4 cm height as illustrated in Fig. 7a. A quartz glass lid provided visibility inside the reactor and the base of the reactor, an aluminum alloy (Al 6061-T6 temper with room temperature thermal conductivity of 167 W/(m.K) [39]), acted as a heat sink in contact with the TE_c, while a layer of silicone heat transfer compound (thermal conductivity of 0.66 W/(m.K), MG Chemicals) was applied between the two. The reactor was then placed on an optical bench which acted as a large heat sink. Two 5 mm inner diameter holes on the glass lid served as an inlet and outlet for the gases. An additional 5 mm diameter hole was used to insert three E-type thermocouples to measure local temperatures. A data acquisition unit (Agilent 34970A) was employed to record the voltage generated by the TE and the surface temperature of the catalyst support. At least 7 runs were done for each testing condition.

The methanol-air mixture, which is assumed to have close to the stoichiometric ratio of methanol to oxygen [1,8,11,13,16], was produced by flowing compressed dry air through methanol in a bubbler. Three air flow rates (112, 165, and 225 sccm) were used. Commercially available platinum nanoparticles (Sigma-Aldrich, USA) with size smaller than 50 nm, confirmed by TEM according to the supplier, were used as catalysts, which

had the specific surface area of 98 m^2/g (Brunauer–Emmett–Teller, BET number). 10 mg

of the Pt nanoparticles were ultrasonically dispersed in 1.5 mL of acetone then drop casted

on top of the 30 ×30 mm area substrate using a pipette and air-dried prior to use. The

schematic of the Pt NPs on the TE is represented in Fig. 1b. The entire setup is

schematically shown in Fig. 7c.
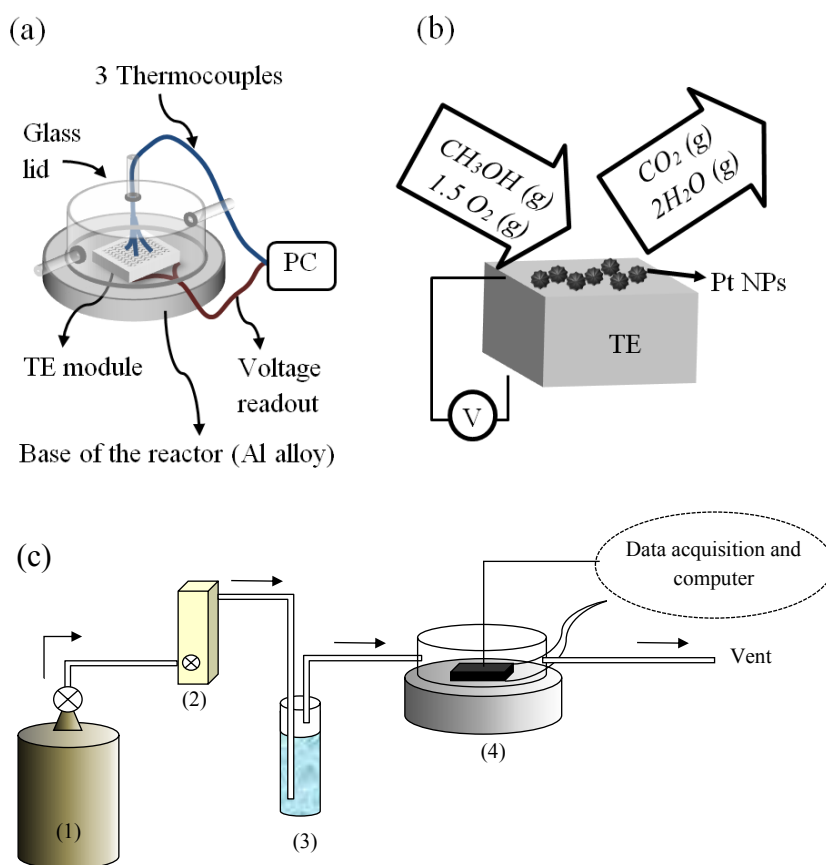
Fig. 7. Schematics of (a) the reactor and (b) Pt NPs on the TE$_h$. (c) Schematic

of the experimental setup: (1) compressed dry air cylinder, (2) flow meter, (3)

bubbler with methanol inside, and (4) reactor with TE module inside.

Three different samples were used in our experiments to study the effect of heat transfer coefficient to TE device: a) Pt nanoparticles deposited directly on the TE_h (Pt-coated TE_h); b) Pt nanoparticles deposited on a 525 micron-thick (100) silicon substrate, which is then placed on the TE_h (Pt-coated Si on TE_h); and c) Pt-coated Si on a glass-slide spacer on the TE_h. Borosilicate glass-slide spacers of thickness 0.14 to 4 mm were tested experimentally. The SEM image of the Pt NPs deposited on the Si substrate is presented in Fig. 8. The image shows that they tend to aggregate on the surface.
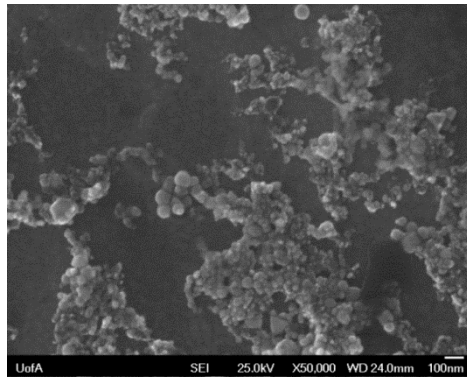
Fig. 8. SEM image of the Pt NPs deposited on the Si substrate.

In order to take the thermal images of the Pt-coated substrate during the experiment, another lid with a 4 cm diameter open window was fabricated. The open window was then covered and sealed by a 5 cm diameter ZnSe window, which is IR transparent. The T640 IR camera (FLIR, USA) with 25° lens was used for thermal imaging.

In order to rationalize the above results, numerical simulations were conducted to evaluate the heat conduction through the composite system (from Pt NPs to aluminum heat sink), using commercially available software, COMSOL Multiphysics. The geometry and size of the of the reactor, TE, inlet and outlet are exactly same as the used ones in experiments. The COMSOL results were obtained by assuming the thermal conductivity of the entire slab of the TE module along with very thin layers of air between each two contact layers on hot and cold side estimated at 1.5 W/m.K. A triangular mesh configuration was used to discretize the geometry in order to solve the heat conduction equation, using 200,000 elements and 40,000 nodal points. The constant input power boundary condition was applied to the Pt coated suface, the value of which is calculated based on the flow rate and assumption of 100% combustion efficiency on the surface. The insulation boundary condition was used for all outer boundaries except on the lower surface of the thermoelectric module where the cold side temperature (T_c) was applied as the boundary condition.

4. Results and discussion

4.1. Experiment results

When Pt nanoparticles were deposited in direct contact with the TE_h, the measured surface temperature rise was less than 0.5°C while the output voltage was 5 mV for a flow rate of 112 sccm. Higher flow rates of 165 and 225 sccm did not result in higher surface temperatures and output voltages, as plotted in Fig. 9a. These results contradict the catalytic combustion results obtained with Pt-coated Si substrate (without a TE module) where the results showed 110°C surface temperatures in the first few minutes for a flow rate of 112 sccm (data not shown). As illustrated in Fig. 9b, when a 0.5 mm-thick Si support was inserted between the Pt NPs and the TE_h, a peak surface temperature of 26.2°C and an output voltage of 135 mV were observed within 30-35 seconds from the start of the experiment using the same flow rate. The readings dropped to 22.8°C and 49 mV within 7 minutes. Qualitatively, the surface temperature and output voltage peak coincided with the appearance of a wet region of approximately 5×5 mm^2 in area, which formed at the center of the Pt-coated Si substrate and began to spread until the entire area was covered in less than a minute, represented in Fig. 9c. Similarly, the peak surface temperatures of 27.1 and 27.9°C were recorded for flow rates of 165 and 225 sccm, respectively, resulting in peak output voltages of 150 and 174 mV, respectively, before decreasing to zero due to catalyst wetting. These results are in agreement with a recent report on water vapor condensation during the nanoburning of methanol reported by Leu et al. [17].
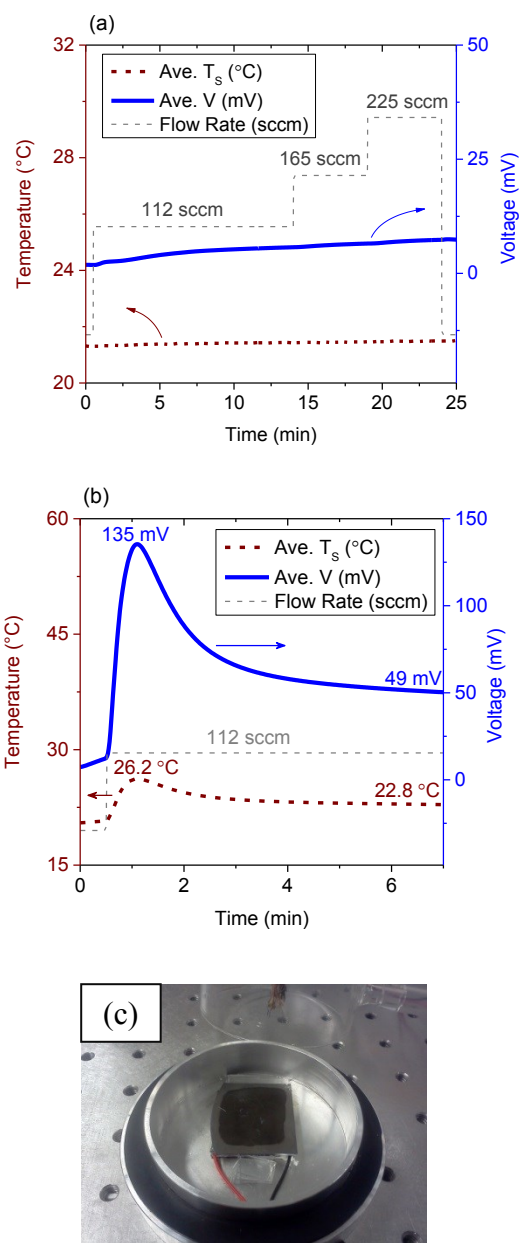
Fig. 9. The variations of the average surface temperature (T_s) on the Si support and the generated TE voltage over time when the catalyst flow rate: (a) Pt-coated TE_h and (b) Pt-coated Si on TE_h at 112 sccm. The real image of the wet Pt-coated Si sample due to condensation of water byproduct. It was in direct contact with TE_h when exposed to methanol-air flow.

When particles are thermally isolated by depositing on quartz wool, as schematically shown in Fig. 10a, CNB is initiated and maintained a high temperature (300-900°C [1,5,8,10-16]) as a result of continuous auto-combustion. However, when there is high heat transfer from nanoparticles to the TE generator, the temperature of the nanoparticles do not reach the threshold temperature needed for the heterogeneous combustion and CNB is inhibited [8] since the catalysts are directly attached to a large heat sink. In the case of Pt-coated Si on TE_h (Fig. 9b), the effective heat transfer coefficient (U_{eff}) of the entire system is reduced when the Si layer is added between the Pt nanoparticles and the TE_h. Heterogeneous catalytic combustion initiated within the first 30 seconds, which was evident from the increased surface temperature and output voltage. However, the U_{eff} is still high enough to cause sufficient heat loss so that enough water vapor condenses on the catalyst to cease the reaction (Fig. 10b). The water vapor, a byproduct of methanol catalytic combustion [1,8,14,17], accumulates on the support as the catalytic combustion proceeds just before the catalyst wetting. Simultaneously, heat is pumped away from the hot side to the cold side of the TE legs, and charge carriers migrate and accumulate at the cold end, which results in a potential difference [34-38]. Thus, heat is dissipated at the same time that the voltage is generated, the Si substrate gets continuously cooled, and water vapor condenses on the relatively cold surface. The expansion of this wet area over the entire surface resulted in a continuous cooling of the support surface and a reduction of active catalyst surface area, leading to a continuous drop in the average surface temperature and generated voltage.

Although effective power generation by inserting a copper heat spreader between a Pt-coated microreactor and a TE module has been reported previously [1,6,20], the data presented in Fig. 9b indicates that effective power generation in these devices may not scale linearly with the thermal conductivity of the spacer. Our results suggest that there should be an optimum value for U_{eff} of the integrated layers in order to maintain high temperatures on the support, prevent the heat sink effect, promote combustion, and prevent water condensation, while providing optimal heat transfer to the TE_h, as shown in Fig. 10c. In the case of the sample with a 1 mm-thick glass-slide spacer (thermal conductivity = 1.05 W/(m.K) [40-42] at room temperature), the effective heat transfer coefficient was reduced enough to result in a constant surface temperature of ~49°C, which is high enough to inhibit water condensation, and produce an output voltage of ~537 mV using 112 sccm flow rate, as illustrated in Fig. 11a. The thermal image of the surface of this sample is represented in Fig. 11b. Both the surface temperature and generated voltage reached a steady state within 3-4 minutes and remain unchanged at constant flow rates even after an extended operation of over 60 minutes. The Si support with high thermal conductivity, 156 W/(m.K) [43] at room temperature, served as a two-dimensional heat spreader while supporting the catalyst nanoparticles.

(a) $CH_3OH_{(g)} + 1.5\ O_{2\ (g)}$

$H_2O_{(g)}$

Thermally isolated Pt NP

$CO_{2\ (g)}$

Quartz microfiber

(b)

$CH_3OH_{(g)}$
$+$
$1.5\ O_{2\ (g)}$

$H_2O_{(l)}$

$CO_{2\ (g)}$

Pt NP

Relatively higher temperature than entire support

Si on TE_h, High U_{eff}

(c)

Radiation (Stefan–Boltzmann's law):
$$Q_{Rad.} = \epsilon \sigma T^4$$

Convection (Newton's law):
$$Q_{Conv.} = h(T - T_\infty)$$

Conduction (Fourier law):
$$Q_{Cond.} = -k_i \frac{\partial T_i}{\partial d_i}$$

Reduced U_{eff} (e.g. Si on glass on TE_h)
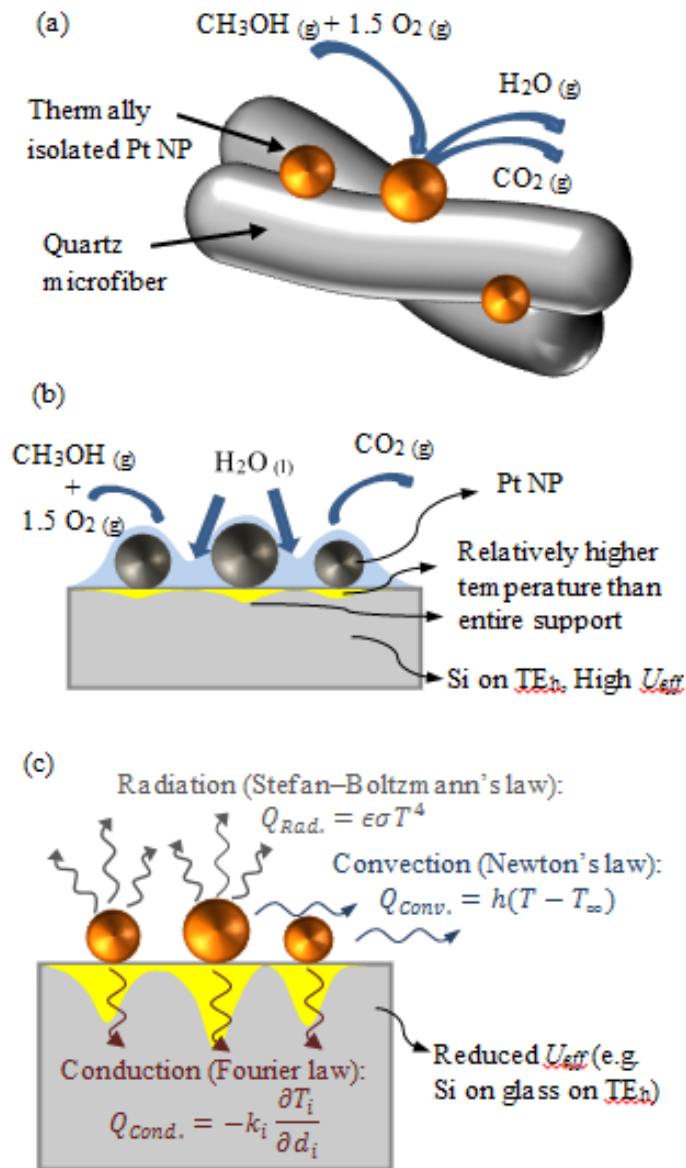
Fig. 10. Schematics of the catalytic combustion behavior of (a) thermally isolated Pt nanoparticles, (b) Pt-coated Si on TE_h, (c) and Pt-coated Si on glass-slide spacer on TE_h.
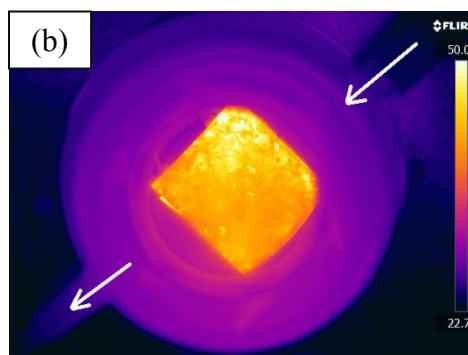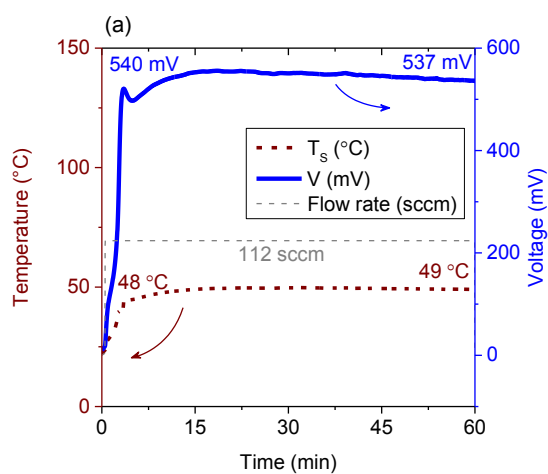
Fig. 11. (a) The variations of the surface temperature (T_s) on Si support and generated voltage by TE over time when glass-slide spacer was interposed between Pt-coated Si and TE_h using 112 sccm flow rate. (b) Thermal image of the Pt-coated Si surface (top view) when 1 mm-thick glass-slide spacer was interposed between the Si support and TE_h and 112 sccm flow rate was used. The white arrows show the inlet-outlet direction and the scale bar shows the range of measured temperature from 22.7 to 50°C.

Although the average support surface temperature was 50-67°C for all tested flow rates when a 1 mm-thick glass spacer was used, there was no evidence of water condensation. The maximum constant output voltage was 1053±45 mV for 225 sccm flow rate. Assuming the TE_c temperature is ~23°C, an output power of ~285 mW was estimated based on the TE resistance of ~4 Ohms, derived from conversion plots provided by the TE manufacturer. Fig. 12 shows the variation of TE resistance by the average surface temperature of the TE sides, which is taken from the specification information of the TE device, provided by the manufacturer for the used TE device, model 1261G-7L31-04CL, Custom Thermoelectric Inc., USA). Having the recorded output voltage (V) for the given flow rate and estimated TE resistance (R_{TE}) based on Fig. 12, the output power (P_{Output}) can be estimated using $P_{Output} = V^2/R_{TE}$ equation.
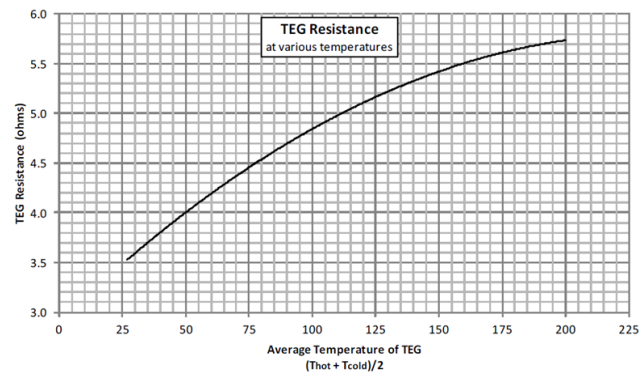
Fig. 12. Variation of the TE resistance by the average surface temperature of the TE sides, provided by the TE manufacturer for TE model 1261G-7L31-04CL, Custom Thermoelectric Inc., USA.

The maximum estimated power conversion efficiency in this research is 2% based on the theoretical combustion power derived from methanol usage at 225 sccm and its low heating value (LHV=639 KJ/mol) [1,31,32]. This efficiency is higher than the 1.1% reported by Karim et al. [1] using a high flow rate of 2000 sccm and a copper spacer.

The explanation can be justified using a heat transfer model, where we assume the radiative heat transfer ($Q_{Rad.}$) is negligible since the catalyst surface temperature is relatively low. Convective heat transfer ($Q_{Conv.}$) is also neglected since the advection flux is small for all the experiments. Therefore, it can be assumed that conductive heat transfer ($Q_{Cond.}$) is the dominant heat transfer mechanism from the catalytic combustion to the graphite foil on the TE$_c$, which is modeled as (per unit area):

$$Q_{cond.} = -k_i \frac{dT_i}{dd_i} = U_{eff}(T_p - T_c) = U_{p-h}(T_p - T_h) \qquad (5)$$

where k_i and d_i represent the thermal conductivity and thickness of the indexed layers, respectively, and $\frac{dT_i}{dd_i}$ is the thermal gradient across its thickness. T_p, T_h, and T_c are the temperature of the Pt NPs, the hot side, and the cold side of TE device, respectively. U_{eff} is the effective heat transfer coefficient between the Pt NPs and the TE$_c$, and U_{p-h} is the heat transfer coefficient between the Pt NPs and the TE$_h$, which are calculated as follows [44]:

$$U_{eff} = \frac{1}{(\frac{d_{Pt}}{k_{Pt}} + \frac{d_{Si}}{k_{Si}} + \frac{d_{Spacer}}{k_{Spacer}} + \frac{d_{TE}}{k_{TE}})} \qquad (6)$$

$$U_{p-h} = \cfrac{1}{(\cfrac{d_{Pt}}{k_{Pt}} + \cfrac{d_{Si}}{k_{Si}} + \cfrac{d_{Spacer}}{k_{Spacer}})} \qquad (7)$$

Since $\frac{d_{TE}}{k_{TE}} \approx 2.14 \times 10^{-3}\ \frac{m^2.K}{W}$, $\frac{d_{Pt}}{k_{Pt}} \approx 7.03 \times 10^{-10}\ \frac{m^2.K}{W}$, and $\frac{d_{Si}}{k_{Si}} \approx 3.21 \times$

$10^{-6}\ \frac{m^2.K}{W}$ are constant, the only variable here is $\frac{d_{Spacer}}{k_{Spacer}}$. The values of U_{eff} and U_{p-h} for

all tested samples, with d_{Spacer} ranging from 0.14 to 4 mm, are calculated from equations

(6) and (7), and presented in Table II. Both U_{eff} and U_{p-h} decrease by adding Si and glass-

slide layers, but the reduction is more pronounced for U_{p-h}. The Pt-coated TE_h, which do

not have the Si support and spacer, showed almost no catalytic activity. It was found that

Pt-coated Si on TE_h, which resulted in the initiation of the catalytic reaction just before

catalyst wetting, has an U_{p-h} approximately 3 orders of magnitude lower than that of Pt-

coated TE_h. However, the heat transfer coefficient of Pt-coated Si on TE_h ($U_{p-h} = 3.11 \times$

10^5 W/m^2.K) was still high enough to induce water formation and quench the CNB

reaction. Insertion of a 0.14 to 4 mm-thick glass-slide spacer between the Pt-coated Si and

the TE_h lowered the U_{p-h} by 2 orders of magnitude, respectively, thereby increasing T_p and

the support surface temperature, eliminating water condensation and sustaining the

catalytic reaction.

Table II. Calculated values of effective heat transfer coefficient between the Pt NPs and the TE_c (U_{eff}) and between the Pt NPs and the TE_h ($U_{p\text{-}h}$)

Sample	d_{Spacer} (mm)	U_{eff} (W/m^2.K)	$U_{p\text{-}h}$ (W/m^2.K)
Pt-coated TE_h	-	466.67	1.42×10^8
Pt-coated Si on TE_h	-	465.97	3.11×10^5
Pt-coated Si on glass slide spacer on TE_h	0.14	438.71	7.32×10^3
	0.22	424.52	4.70×10^3
	0.44	389.85	2.37×10^3
	1	322.74	1.05×10^3
	2	246.86	0.52×10^3
	3	199.87	0.35×10^3
	4	167.91	0.26×10^3

Fig. 13 represents the effects of spacer thickness and air flow rates through a methanol bubbler on the average support surface temperature (Fig. 13a) and generated voltage (Fig. 13b). The highest output voltage and power were resulted from the 1 mm-thick glass-slide spacer. Increasing the thickness of the spacer from 1 to 4 mm decreases the $U_{p\text{-}h}$ value by a factor of ~4 (Table I), which lowers heat transfer rate to the TE_h. Experimental results, which are represented in Fig. 13, show the higher support surface temperature but a lower T_h on the hot side of the TE when spacer thickness increases from 1 to 4 mm. Lowering the spacer thickness from 1 to 0.14 mm resulted in ~7 times increase in $U_{p\text{-}h}$ value and more efficient heat dissipation through the TE composite slab thickness to TE to heat sink. Therefore, both of the support surface temperature and T_h were decreased, which is evident from Fig 13a and b, respectively. In case of no glass slide spacer, the heat dissipation was

high enough to keep the catalyst support temperature cold enough to induce water vapor condensation as discussed before (Fig. 9).

The relationship between the average TE output voltage and support surface temperature is shown in Fig. 13c at different flow rates. The lower surface temperatures are achieved by using lower spacer thicknesses for the tested flow rates, while higher flow rates at given spacer thickness increases both the voltage and the surface temperature. These plots confirm the possibility of getting a higher output voltage and power using an optimum thickness of the glass-slide spacer in the range of 0.44 to 1 mm, while still preventing water vapor condensation. These results suggest the optimum heat transfer coefficient, $U_{p\text{-}h}$, of $1.05 - 2.37 \times 10^3$ (W/m^2.K) for the proposed integrated power source, which leads to the highest possible output voltage, power, and efficiency.
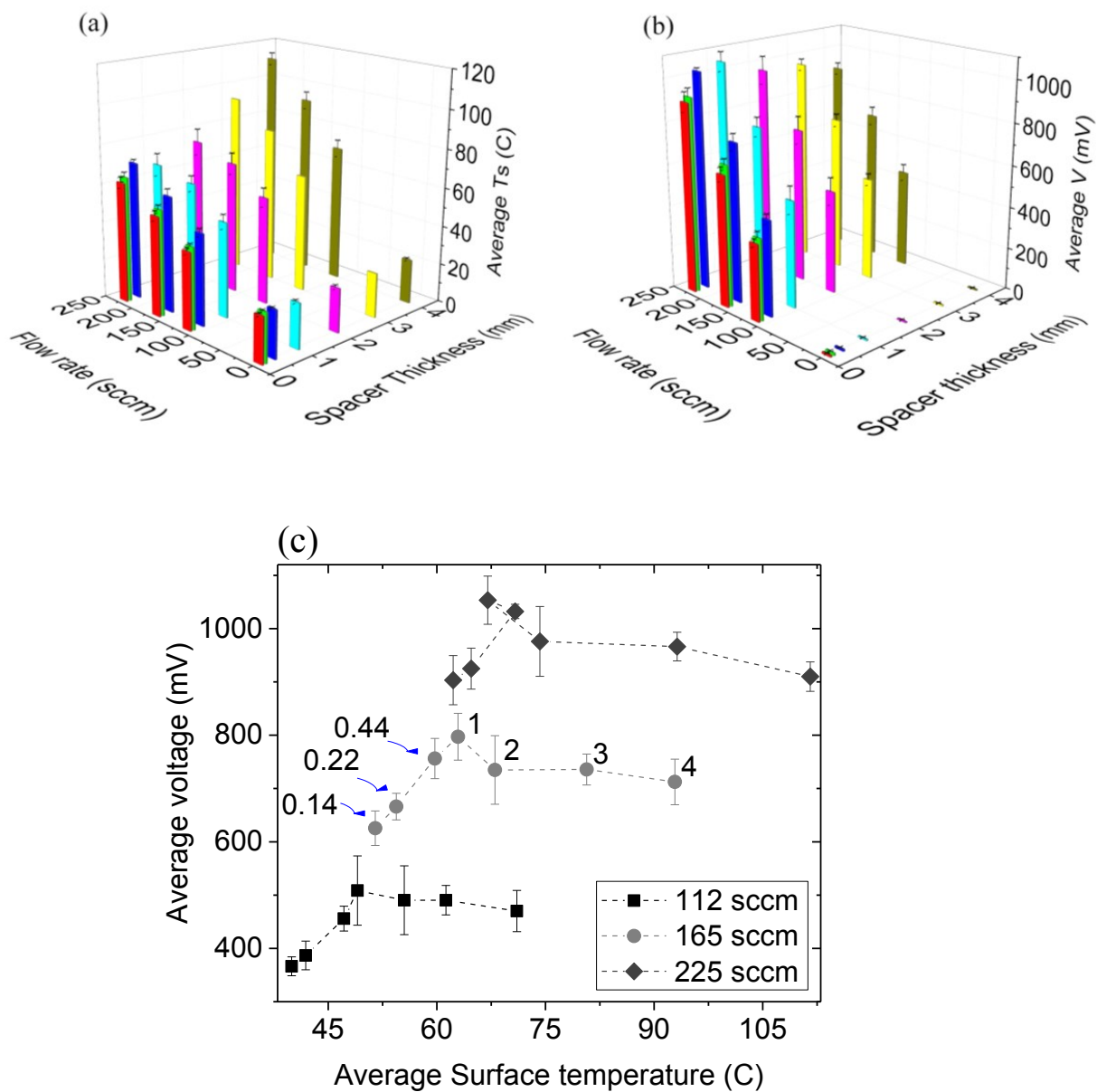
Fig. 13. (a) Variations of the average surface temperature on the support and (b) generated voltage by TE with flow rate and glass-slide spacer thickness. (c) Variations of average generated voltage with average surface temperature on the Si support resulted from different glass-slide spacer thicknesses (in mm), noted above each data point, for different flow rates.

Not surprisingly, the support surface temperature increases as the spacer thickness increases from 1 to 4 mm for any flow rate. Conversely, the average generated voltage decreases as the spacer thickness increases, which is consistent with a lower T_h as a result of reduced U_{p-h}. For example, for a flow rate of 225 sccm, the average surface temperature increased from 67±6 to 112±3°C and the average generated voltage decreased from 1053±45 to 910±28 mV as the spacer thickness was increased from 1 to 4 mm. Fig. 13 indicates that increasing the methanol-air flow rate at any given spacer thickness increases the support surface temperature (Fig. 13a) and the hot side temperature (Fig. 13b), the latter being inferred from the increased output voltage. Higher catalyst surface temperatures with higher reactant flow rates has been previously reported, which is the result of the higher combustion rate [1,3,4,6,8,10-14,16,18,20,23,31,32]. With more fuel entering the hot reactor per unit time, there is more combustion, and therefore, more heat released per unit of time, which is defined as the input power [6,16,23,31,32]. In addition, monitoring the methanol usage revealed that the O_2/methanol ratio increases from 1.28 to 1.43 to 1.54 as the flow rate was increased from 112 to 165 to 225 sccm, respectively, which confirms the possibility of more efficient combustion at higher flow rates as a result of an increase in the O_2/fuel ratio to stoichiometric mixture [13,16].

4.2. COMSOL model results

A computer-based model was used to check the trustworthiness of the experimental results and predict the behavior of the system at wider range of heat transfer coefficients of the spacer material. COMSOL Multiphysics software was used and the conjugate heat transfer module was applied, which involves all modes of heat transfer, to optimize the thermal conductivity and the thickness of the spacer intervening the Pt catalyst support and the hot side of the TE device. The local temperature values on Si support (T_s) and TE hot side (T_h) are calculated by solving the heat transfer equations in COMSOL, assuming the steady heat conduction rate per unit area, $Q_{Cond.}$, across the thickness of the composite layers of Si support, spacer, and TE. The $Q_{Cond.}$ is calculated based on the flow rate and low heating value of the fuel. The simulated values of T_s and T_h are resulted, which are the average temperature values over the Pt-coated substrate and the hot side of TE module, respectively.

Fig. 14a represents the simulated vortex flow inside the reactor when the flow rate of 165 sccm was used. The estimated residence time is 43-86 seconds for the flow rates of 112 to 225 sccm, which is long enough to suggest the probability of complete combustion and constant heat release. Heat release, which defines the input power, can be assumed constant, provided that the heat transfer coefficient is not high enough to quench the reaction and lower the combustion efficiency. Figs. 14b, c, and d show the temperature profile inside the rector and across the thickness of the composite slab for different thicknesses of the glass slide spacer.
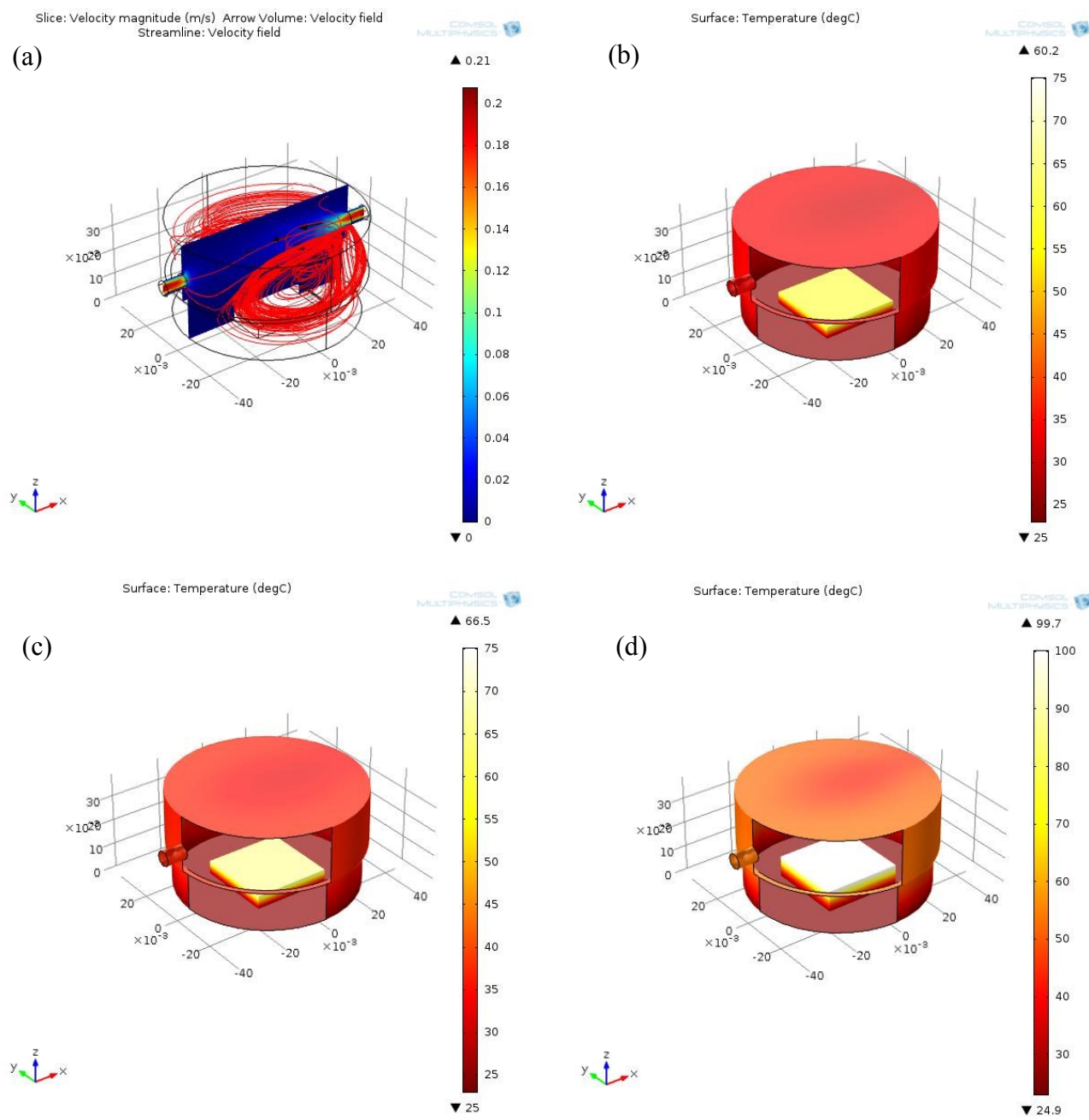
Fig. 14. COMSOL simulation images of the modeled CNB reactor at 165 sccm flow rate, corresponding to 11 W input power: (a) streamlines showing the vortex flow inside the reactor, (b), (c), (d) the thermal image of the composite slab inside the reactor for the glass-slide spacer thickness of 0.44, 1 and 4 mm, respectively.

In order to achieve the objective of simulation, a wide range of heat transfer coefficients and thicknesses of the spacer material were evaluated. The simulation results reveal that decreasing the d_{Spacer}, which is inversely increasing the U_{Spacer}, result in surface temperature (T_s) reduction dramatically, whereas the temperature of the TE hot side (T_h) increases slightly. The value of T_h actually determines the value of generated voltage by TE. The higher the T_h is, the higher voltage generation by the TE module will be. Fig. 15a represents the simulated variation of T_s and T_h as a function of d_{Spacer} and Fig. 15b plots those T_s variations with respect to T_h, while the input power of 11 W was applied, corresponding to the flow rate of 165 sccm.

Inspection of Fig. 15 reveals that decreasing the thickness of the spacer results in decreasing the Pt-coated surface temperature (T_s), and at the same time, increasing the hot side temperature (T_h), which means possibility of getting higher voltage by TE. These plots confirm the experimental results for the range of 1-4 mm-thick glass-slide spacer, which was presented in section 4.1. Decreasing the T_s and increasing T_h by means of the increase of the heat transfer coefficient value of the spacer material (U_{glass}) is confirmed by the modeled values presented in Fig. 15. The modeled values of T_s and T_h for the range of 1-4 mm-thick glass-slide spacer, presented in Fig. 15, are very close to those acquired experimentally, which are presented in Fig 13. However, this model is not working thoroughly if lower than 1 mm glass-slide spacer is modeled.
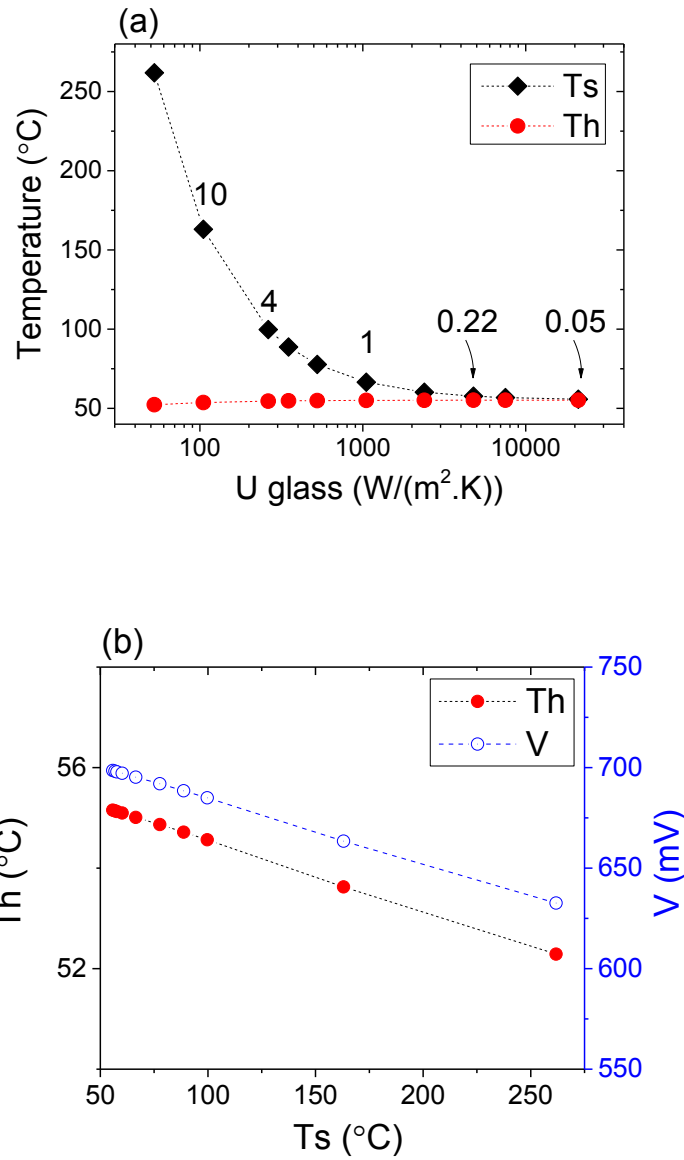
Fig. 15. Plots resulted from COMSOL model: (a) variation of the temperature on the catalyst support (T_s) and TE hot side (T_h) by heat transfer coefficient of the spacer (U_{glass}), and (b) variation of TE hot side temperature (T_h) and output voltage by catalyst support temperature (T_s). The numbers above each data point shows the thickness of the spacer.

To justify why the COMSOL model is working very good for the spacer thicknesses of above 1 mm and not predicting the right results for the thicknesses of below 1, one should keep it in mind that the constant power heat source is used for this modeling, while in reality, the heat source is not releasing the constant input power when thicknesses of the spacer is falling below 1 mm. The CNB reaction is the heat source, which is quenched when the thickness of the glass-slide spacer is below 1 mm as discussed in section 4.1 and represented in Fig. 13. To overcome this problem, a more developed model is suggested to be used, which can predict the heat release rate of the catalytic reaction based on flow rate of reactants and adsorption/desorption rate of the water vapor byproduct based on the catalyst surface temperature.

5. Conclusions

In summary, the present study shows the importance of the effective heat transfer coefficient of the sandwiched layers in an integrated CNB and TE generator in order to prevent the heat sink effect and water condensation and to sustain the catalytic reaction. The use of a 0.44-1 mm-thick glass-slide spacer between the 0.5 mm-thick catalyst support and TE, which offers the heat transfer coefficient, U_{p-h}, of 1.05– 2.37 $\times$ 10^3 (W/m^2.K) between the catalyst nanoparticles and TE_h, led to the best results. It resulted in the maximum average output voltage of 1053 mV at 225 sccm flow rate and maximum output power of ~285 mW when the thickness of the glass-slide spacer was 1 mm. The estimated maximum power conversion efficiency is 2%. Thermal management by adjusting the $\frac{d_{Spacer}}{k_{Spacer}}$ value to satisfy the U_{p-h} is a critical step in the successful fabrication of integrated, handheld, and portable power devices. However, further optimization studies are required, coupled with simulations, to pin-point the exact thermal properties of the integrated system.

COMSOL Multiphysics software is used to model the experimented system and the properties and dimensions of the model are same as the tested values. The constant input power corresponding to the applied flow rate is used in a conjugate heat transfer module. This model predicts the temperatures of the catalyst surface (T_s) TE hot side (T_h) very close to the experimental values if 1 mm or thicker glass-slide spacer is modeled. However, the model is not reliable for the spacer thicknesses of below 1 mm, since the CNB is getting quenched and the power input is not constant anymore. The experimental

data has shown that the power input dropping when the thickness of the glass slide spacer is below 1 mm. A more sophisticated model which can predict the combustion efficiency based on the flow rate and adsorption/desorption rate of the water vapor base on the catalyst temperature should be developed in order to model the setup thoroughly at all spacer thicknesses and heat transfer coefficients.

References

[1]   A. M. Karim, J. A. Federici, and D. G. Vlachos, Journal of Power Sources **179**, 113 (2008).

[2]   C. H. Marton, G. S. Haldeman, and K. F. Jensen, Industrial & Engineering Chemistry Research **50**, 8468 (2011).

[3]   D. E. Park, T. Kim, S. Kwon, C. K. Kim, and E. Yoon, Sensors and Actuators a-Physical **135**, 58 (2007).

[4]   J. Jin and S. Kwon, International Journal of Hydrogen Energy **35**, 1803 (2010).

[5]   J. D. Holladay, E. O. Jones, M. Phelps, and J. L. Hu, Journal of Power Sources **108**, 21 (2002).

[6]   J. A. Federici, D. G. Norton, T. Bruggemann, K. W. Voit, E. D. Wetzel, and D. G. Vlachos, Journal of Power Sources **161**, 1469 (2006).

[7]   I. Glassman and R. A. Yetter, *Combustion* (Elsevier, USA, 2008), 4 edn., p.^pp. 653.

[8]   Z. Hu, V. Boiadjiev, and T. Thundat, Energy & Fuels **19**, 855 (2005).

[9]   M. Haruta, A. Ueda, S. Tsubota, and R. M. T. Sanchez, Catalysis Today **29**, 443 (1996).

[10]   J. R. Applegate, H. Pearlman, and S. D. Bakrania, Journal of Nanomaterials, 460790 (2012).

[11]   D. Resnik, S. Hocevar, J. Batista, D. Vrtacnik, M. Mozek, and S. Amon, Sensors and Actuators a-Physical **180**, 127 (2012).

[12]   C. H. Leu, S. C. King, C. C. Chen, J. M. Huang, S. S. Tzeng, I. H. Liu, and W. C. Chang, Applied Catalysis a-General **382**, 43 (2010).

[13]   Y. Ma, C. Ricciuti, T. Miller, J. Kadlowec, and H. Pearlman, Energy & Fuels **22**, 3695 (2008).

[14]   O. J. Kwon, D. H. Yoon, and J. J. Kim, Chemical Engineering Journal **140**, 466 (2008).

[15]   K.-F. Lo and S.-C. Wong, Journal of Power Sources **213**, 112 (2012).

[16]   J. R. Applegate, D. McNally, H. Pearlman, and S. D. Bakrania, Energy & Fuels **27**, 4014 (2013).

[17]   C. H. Leu, S. C. King, J. M. Huang, C. C. Chen, S. S. Tzeng, C. I. Lee, W. C. Chang, and C. C. Yang, Chemical Engineering Journal **226**, 201 (2013).

[18]   T. Kim, International Journal of Hydrogen Energy **34**, 6790 (2009).

[19]   M. Ditaranto, J. E. Hustad, T. Slungaard, and A. H. Briand, Energy & Fuels **21**, 1982 (2007).

[20]   D. G. Norton, E. D. Wetzel, and D. G. Vlachos, Industrial & Engineering Chemistry Research **45**, 76 (2006).

[21]   D. G. Norton and D. G. Vlachos, Proceedings of the Combustion Institute **30**, 2473 (2005).

[22]   D. G. Norton, E. D. Wetzel, and D. G. Vlachos, Industrial & Engineering Chemistry Research **43**, 4833 (2004).

[23]   S. Bensaid, M. Brignone, A. Ziggiotti, and S. Specchia, International Journal of Hydrogen Energy **37**, 1385 (2012).

[24]   S. b. A. Design Institute for Physical Properties, (Design Institute for Physical Property Research/AIChE, NY, USA, 2012).

[25]   C. L. Yaws, *Yaws' Handbook of Thermodynamic and Physical Properties of Chemical Compounds* (Knovel, NY, USA, 2003), 2003 edn.

[26]   D. E. Park, T. K. Kim, S. Kwon, and E. Yoon, in *MEMS 2006: 19th IEEE International Conference on Micro Electro Mechanical Systems, Technical Digest*Istanbul, Turkey, 2006), pp. 942.

[27]   D. E. Park, T. K. Kim, S. Kwon, C. K. Kim, and E. Yoon, in *4th International Conference on Fuel Cell Science, Engineering, and Technology*Irvine, CA, USA, 2006), pp. 1001.

[28]   T. Kim, S. Kwon, and Asme, in *IMECE 2008: ASME International Mechanical Engineering Congress and Exposition*Boston, MA, USA, 2008), pp. 345.

[29]   W. Shin, T. Nakashima, M. Nishibori, T. Itoh, N. Izu, I. Matsubara, Y. Nakagawa, A. Yamamoto, and H. Obara, Journal of Electronic Materials **40**, 817 (2011).

[30]   W. Shin, T. Nakashima, M. Nishibori, N. Izu, T. Itoh, and I. Matsubara, Current Applied Physics **11**, S36 (2011).

[31]   J. Vican, B. F. Gajdeczko, F. L. Dryer, D. L. Milius, I. A. Aksay, and R. A. Yetter, Proceedings of the Combustion Institute **29**, 909 (2002).

[32]   K. Yoshida, S. Tanaka, S. Tomonari, D. Satoh, and M. Esashi, Journal of Microelectromechanical Systems **15**, 195 (2006).

[33]   D. E. Park, T. K. Kim, S. Kwon, C. K. Kim, and E. Yoon, *Micromachined methanol steam reforming system integrated with catalytic combustor using carbon nanotubes as catalyst supports* 2006), Proceedings of the 4th International Conference on Fuel Cell Science, Engineering, and Technology.

[34]   F. J. DiSalvo, Science **285**, 703 (1999).

[35]   S. B. Riffat and X. L. Ma, Applied Thermal Engineering **23**, 913 (2003).

[36]   G. Chen, M. S. Dresselhaus, G. Dresselhaus, J. P. Fleurial, and T. Caillat, International Materials Reviews **48**, 45 (2003).

[37]   A. J. Minnich, M. S. Dresselhaus, Z. F. Ren, and G. Chen, Energy & Environmental Science **2**, 466 (2009).

[38]   G. J. Snyder and E. S. Toberer, Nature Materials **7**, 105 (2008).

[39]   *Properties and selection: nonferrous alloys and special-purpose materials, ASM Handbook* (ASM Iternational, 1991), 10 edn., Vol. 2, ASM Handbook, p.^pp. 62-122.

[40]   W. M. Haynes, *"Thermal conductivity of glasses," in CRC Handbook of Chemistry and Physics* (CRC Press/Taylor and Francis, Boca Raton, FL, 2014).

[41]   R. Baboian, *NACE Corrosion Engineer's Reference Book (3rd Edition)* (NACE International, Houston, TX, 2002).

[42]   C. L. Yaws, *Yaws' Critical Property Data for Chemical Engineers and Chemists* (Knovel, NY, USA, 2012), 2012 edn.

[43]   C. J. Glassbrenner and G. A. Slack, Physical Review **134**, A1058 (1964).

[44]   J. P. Holman, *Heat transfer* (McGraw Hill Higher Education, Boston, 2010), 10th edn., McGraw-Hill series in mechanical engineering.